ADVANCED ENERGY MATERIALS
www.advenergymat.de

Doping-Induced Screening of the Built-in-Field in Organic Solar Cells: Effect on Charge Transport and Recombination

*Ardalan Armin, Gytis Juska, Bronson W. Philippa, Paul L. Burn, Paul Meredith, Ronald D. White, and Almantas Pivrikas**

We report on the effects of screening of the electric field by doping-induced mobile charges on photocurrent collection in operational organic solar cells. Charge transport and recombination were studied using double injection (DI) and charge extraction by linearly increasing voltage (CELIV) transient techniques in bulk-heterojunction solar cells made from acceptor-donor blends of poly(3-*n*-hexylthiophene):phenyl-C61-butyric acid methyl ester (P3HT:PC60BM). It is shown that the screening of the built-in field in operational solar cells can be controlled by an external voltage while the influence on charge transport and recombination is measured. An analytical theory to extract the bimolecular recombination coefficient as a function of electric field from the injection current is also reported. The results demonstrate that the suppressed (non-Langevin) bimolecular recombination rate and charge collection are not strongly affected by native doping levels in this materials combination. Hence, it is not necessary to reduce the level of doping further to improve the device performance of P3HT-based solar cells.

1. Introduction

Organic semiconductors are promising materials for low-cost, printable, portable and flexible solar cells and a variety of other optoelectronic devices.[1–6] Recent developments in organic solar cells (OSCs) prepared from blends of conjugated polymers and fullerene derivatives have led to significant improvements with power conversion efficiencies (PCE) now exceeding 10%.[7–9] It has been shown that the performance of OSCs is heavily influenced by a variety of defects which adversely affect transport, carrier recombination and the exciton diffusion length.[10] For example, the destructive effects of oxygen exposure on poly(3-*n*-hexylthiophene):phenyl-C61-butyric acid methyl ester (P3HT:PC60BM) devices are caused by defect-induced equilibrium charge carriers as reported by Schafferhans et al.[11] However, the influence of such defects and "impurities" might not always be negative. For example, Liu et al[12] have shown that the efficiency of perylene diimide and phthalocyanine-based devices drops when the materials are purified. Since bulk material costs critically depend upon purity requirements, a detailed knowledge of such effects are of particular importance as we move towards large scale OSC manufacturing.

In this regard, the role of impurities on photovoltaic performance has been previously studied by a variety of techniques including: analysis of the current-voltage characteristics;[13,14] charge transport measurements;[10,11] and a qualitative study of carrier recombination.[15] The role of impurities has also been studied in a number of materials, for example: chemical doping in copper phthalocyanine (CuPc):PC60BM devices;[13] rubrene doping in zinc phthalocyanine (ZnPc):PC60BM solar cells;[14] and in 5,5′-bis{(4-(7-(5-hexylthiophen-2-yl))thiophen-2-yl)[1,2,5]thiadiazolo[3,4-*c*]pyridine}-3,3′-di-2-ethylhexylsilylene-2,2′-bithiophene:[6,6]-phenyl-C_{71}-butyric acid methyl ester [*p*-DTS(PTTh$_2$)$_2$:PC$_{70}$BM] blends.[15] The influence of defects specifically on carrier mobility in P3HT:PCBM solar cells has also been investigated.[10,11] However, since the charge collection efficiency is controlled by charge transport and recombination,[16] it is essential to consider simultaneously both carrier mobility and carrier lifetime in operational devices where the built-in electric field is partially screened.[17]

While the intrinsic, thermally generated mobile carrier concentration is expected to be low (<10^5 cm^{-3}) in pristine organic semiconductors due to their large bandgap (typically exceeding 1.8 eV), the actuality is that much higher carrier concentrations have been detected in typical films of polymers such as P3HT.[17] These so called "dark carriers" have been variously thought to arise from impurities (typically not as high as inorganic crystals), structural disorder, and/or oxygen and/or water based doping. In general it is common to use the word "doping" to describe defects or impurities deliberately incorporated into the semiconductor. However, by analogy with inorganic

A. Armin, Prof. P. L. Burn, Prof. P. Meredith, Dr. A. Pivrikas
Centre for Organic Photonics & Electronics (COPE)
School of Chemistry and Molecular Biosciences and School of Mathematics and Physics
The University of Queensland
Brisbane 4072, Australia
E-mail: a.pivrikas@uq.edu.au
B. W. Philippa, Prof. R. D. White
School of Engineering and Physical Sciences
James Cook University
Townsville 4811, Australia
Prof. G. Juska
Department of Solid State Electronics
Vilnius University
10222 Vilnius, Lithuania

DOI: 10.1002/aenm.201200581

semiconductors, we will adopt the nomenclature of using the word "doping" to describe those unbound electrically charged defects (arising from any non photo-induced means) providing mobile electrons or holes. The equilibrium charge carriers created by these dopants will respond to the built-in electric field of the solar cell, causing a depletion layer. It has been shown that such doping creates a Schottky diode, and a field-free region across the film.[18,19] Morfa et al[17] have shown that in very thick P3HT:PCBM solar cells with moderate doping ($n = 5 \times 10^{15}$ cm^{-3}), at low bias voltages charge transport occurs via diffusion because the built-in field is screened by the charge caused by the doping. This phenomenon results in low power conversion efficiencies, since screening of the built-in field has a negative effect on photocurrent collection due to recombination losses.[20,21] The recombination losses can be due to either first order (carrier density independent) or higher order (density dependent)[22] recombination of excitons, charge transfer states, polaron pairs and free charge carriers. Regardless of the recombining species, the impact of the recombination will reduce collection efficiency. Even though first order recombination is present even at low densities, it is independent of charge carrier concentration. Higher order recombination becomes an actual problem when the extraction rate is low because the lifetime is density dependent.

In general, it is expected that Langevin type bimolecular recombination will be observed in organic semiconductors[23] due to the short carrier hopping distances (low mobility materials) in comparison to the Coulomb escape radius.[24] Non-Langevin recombination, wherein the bimolecular recombination is suppressed relative to the Langevin limit, is observed in annealed P3HT:PCBM solar cells[24] and other blends.[26,27] Non-Langevin materials can support higher carrier densities, leading to larger extraction and injection currents, and thus improved device performance.[28,29] It has been shown previously that lossless carrier extraction may occur if $\mu_{slower}\beta_L/\beta$ is sufficiently large, where μ_{slower} is the mobility of the slower carriers, and β_L/β is the bimolecular recombination reduction factor[28] (the ratio of the Langevin rate β_L to the actual rate β). Therefore, by measuring the slower carrier mobility and the bimolecular recombination reduction factor, one can determine whether or not the performance of a given organic solar cell is limited by charge collection efficiency. This is the approach we adopt in this current work to study the impacts of the electic field screening on the charge collection efficiency in efficient P3HT:PCBM cells. We use Charge Extraction under Linearly Increasing Voltage (CELIV), photo-CELIV and double injection techniques to show that bulk-heterojunction (BHJ) cells can operate in two different conductivity regimes depending on the applied external voltage in relation to the doping level of the active film. We present a theory by which it is possible to calculate the bimolecular recombination coefficient from double injection (DI) experiments (i.e., in the dark) in both conductivity regimes, and using the same method extract the carrier mobilities over the whole range of electric fields applicable to operational devices. We have also measured the bimolecular recombination rate using photo-CELIV[30] and good agreement between both techniques is observed. Critically, the results show that the power conversion efficiency in efficient P3HT:PCBM blends is not limited by charge transport and recombination because the majority of photogenerated charges are extracted prior to recombination. This is achieved though a sufficiently high extraction rate as well as through slow (non-Langevin) recombination. As long as power conversion efficiency is not limited by charge collection efficiency due to doping, we would expect no improvement in performance by reducing the doping level. This fits with large amounts of historical, empirical data and experience with P3HT which indicate that over and above a reasonable level of purity the material is remarkably robust despite an apparent high dark carrier density.

2. Theory and Simulations

In this section, we present a method for measuring the bimolecular recombination reduction factor β_L/β from a double injection (DI) experiment. We will show that there are two distinct experimental regimes, which we call the high conductivity and the low conductivity regimes. These regimes are distinguished by the ratio of the total amount of equilibrium majority charge carriers (Q_0) compared to the steady state charge on the electrodes (CU). The doped semiconductor film itself has a neutral charge, because mobile carriers possess one type of charge (for instance positive) while dopants possess the opposite (negative charge). These mobile charge carriers and dopants compensate each other and create charge neutrality in the film. The electrodes have an additional charge which is determined by the applied voltage and device capacitance (CU). Depending on the relative magnitude of the total film charge (Q_0), the electric field inside the film will either be fully screened ($Q_o > CU$) or unscreened ($Q_o < CU$).

The low conductivity regime, described as injection into an insulator, has $Q_0 < CU$; while the high conductivity regime, described as injection into a semiconductor, has $Q_0 > CU$.[31] Equivalently, these regimes may be described by the ratio of the small signal transit time $t_{tr} = d^2/\mu U$ (where d is the device thickness and μ the majority carrier mobility) to the dielectric relaxation time $\tau_\sigma = \varepsilon\varepsilon_0/\sigma$ (where $\varepsilon(\varepsilon_0)$ is the relative (vacuum) permittivity, and σ its conductivity). The low conductivity case has $t_{tr} < \tau_\sigma$, whereas the high conductivity case has $t_{tr} > \tau_\sigma$. The theory of double injection in semiconductors and insulators has been extensively studied.[29–31]

DI current transients are recorded by applying a square-shaped voltage in forward bias to the device. When the bimolecular recombination coefficient is much less than the Langevin coefficient, the carrier density in the film (and hence the current) increases with time due to plasma formation,[33] and reaches values much higher than the initial injection current. At times greater than the transit time, the current finally saturates to j_{DI} (the double injection steady state current) due to carrier recombination. In the case of double injection into insulators with a low bimolecular recombination coefficient, two "kinks" are predicted in the transient, as shown in **Figure 1**a. The first kink represents the time at which the faster and slower carriers meet, and recombination begins. Recombination causes the current to decrease as carriers are lost. Computer simulations show that the faster carrier transit time (t_{fast}) coincides with the zero in the derivative of the current transient (refer to Figure 1a). The second kink, t_{slow}, marks the transit time of slower carriers.

DOI: 10.1002/aenm.201200581

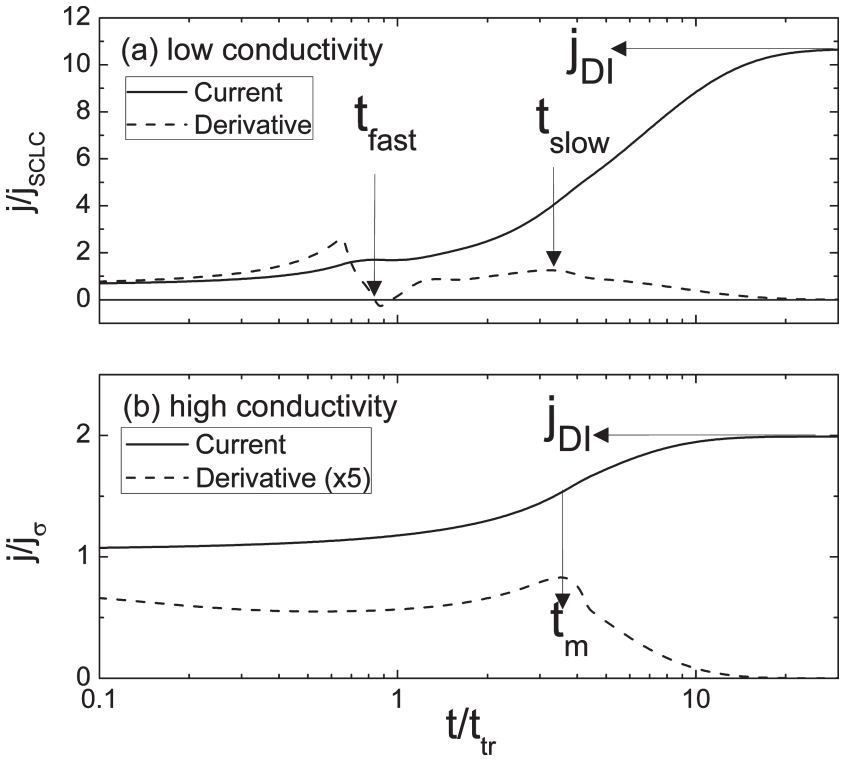

Figure 1. Simulated double injection current transient responses from numerical solution of the continuity equations and Poisson's equation demonstrating the typical features used to obtain transport and recombination parameters. (a) double injection into a low conductivity film, with $\frac{Q_0}{CU} = \frac{t_{tr}}{\tau_\sigma} = 0.1$ where Q_0 is equilibrium charge, C capacitance of the device, U applied voltage, t_{tr} carrier transit time and τ_σ dielectric relaxation time; and (b) double injection into a high conductivity film, with $\frac{Q_0}{CU} = \frac{t_{tr}}{\tau_\sigma} = 10$, where Q_0 is the amount of doping-induced equilibrium charge carriers in the film. Solid lines show the injection current transient signal whereas the dashed line represents the time-derivative. The low conductivity transient shows two transit times, $t_{fast}(t_{slow})$ for faster (slower) carriers; whereas the high conductivity transient shows only one characteristic time t_m, which corresponds to the ambipolar carrier transit time. The steady state injection current (typically recorded from current-voltage measurements) is shown as j_{DI}. The bimolecular recombination coefficient used in the simulations was $\beta = \beta_L/100$ (where β_L is the Langevin rate), and the mobility ratio is $\mu_{faster} = 5\mu_{slower}$ [where μ_{faster} (μ_{slower}) is the mobility of the faster (slower) carriers]. Ideal (Ohmic) boundary conditions were used, and RC circuit effects, trapping and monomolecular recombination were neglected.

$$j_{DI} = \varepsilon\varepsilon_0\sqrt{\frac{9\pi}{8}}\sqrt{\frac{\mu_p\mu_n(\mu_p+\mu_n)}{\mu_R}}\frac{U^2}{d^3}, \quad (1)$$

where j_{DI} is the steady state DI current, $\mu_R = \frac{\varepsilon\varepsilon_0\beta}{2e}$, e the electron charge, β bimolecular recombination, U the forward bias voltage, d the film thickness and μ_n (μ_p) electron (hole) mobility. If the recombination is defined by the Langevin rate β_L (where $\beta_L = \frac{e(\mu_p+\mu_n)}{\epsilon\epsilon_0}$), the total current is the sum of pure electron and hole space charge limited currents, as shown by Lampert and Mark,[31,32] (Equation 11.37)

$$j_{SCLC} = \frac{9\varepsilon\varepsilon_0(\mu_p+\mu_n)U^2}{8d^3}. \quad (2)$$

Using $\beta_L = \frac{e(\mu_p+\mu_n)}{\varepsilon\varepsilon_0}$, and Equation (1) and (2) we can write

$$\frac{\beta_L}{\beta} = C\left(\frac{j_{DI}}{j_{SCLC}}\right)^2, \quad (3)$$

where

$$C = \frac{9}{16\pi}\frac{(\mu_p+\mu_n)^2}{\mu_p\mu_n}.$$

Using Equation (3), and measuring j_{DI} and j_{SCLC} experimentally from current transient signals (Figure 1a), allows one to obtain the bimolecular recombination reduction factor $\frac{\beta_L}{\beta}$ in the low conductivity regime. The coefficient C is defined by the ratio of electron and hole mobilities. For different mobility ratios here are some examples of the coefficient C:

$$\mu_n = \mu_p \Rightarrow C = 0.71,$$

$$\mu_n = 3\mu_p \Rightarrow C = 0.95,$$

$$\mu_n = 10\mu_p \Rightarrow C = 2.16.$$

The case of double injection into a semiconductor is shown in Figure 1b. There is only one kink (t_m) in the transient, which corresponds to the ambipolar (minority) carrier transit time. This is because in a high conductivity material, majority carriers already exist in equilibrium in the film, so these carriers begin to move immediately when the voltage is applied.

Based upon this qualitative framework, we derive analytical equations to extract the bimolecular recombination coefficient from double injection transients in the case of injection into insulators and semiconductors at steady state.

2.1. Calculation of the Bimolecular Recombination Coefficient in the Low Conductivity Regime

Double injection of steady state current into an insulator has an exact analytical solution as shown by Lampert and Mark,[31] (Equation 11.35)

2.2. Calculation of the Bimolecular Recombination Coefficient in the High Conductivity Regime

The saturation current resulting from double injection into a semiconductor (in the case of high film conductivity) also has an exact analytic solution, as shown by Lampert and Mark,[31] (Equation. 12.19)

$$j_{DI} = \frac{8}{9}e\mu_p\sqrt{\frac{(b+1)\mu_n(n_0-p_0)}{\beta}}\frac{U^{3/2}}{d^2}, \quad (4)$$

where $b = \frac{\mu_n}{\mu_p}$ and $n_0(p_0)$ is the thermally generated equilibrium electron (hole) concentration. The ambipolar transit time is given by

$$t_a = \frac{L^2}{\mu_a U}, \quad (5)$$

where the ambipolar (minority) carrier mobility is $\mu_a = \frac{\mu_n \mu_p (n_0 - p_0)}{n_0 \mu_n + p_0 \mu_p}$.

The Ohmic injection current is the sum of majority and minority charge carrier currents

$$j_\sigma = e\left(n_0 \mu_n + p_0 \mu_p\right) \frac{U}{d}. \quad (6)$$

Using Equations (4)–(6) we get

$$\frac{\beta_L}{\beta} = C\left(\frac{j_{DI}}{j_\sigma}\right)^2, \quad (7)$$

where $C = \frac{81}{64} \frac{t_a}{\tau_\sigma}$, which is applicable to the case of the high conductivity regime. Experimentally, the ambipolar transit time, t_a can be measured from double injection current transients[34] and the dielectric relaxation time τ_σ is measured from the dark CELIV experiment.[35]

3. Results

The dark CELIV technique was used to measure the doping-induced mobile charge carrier concentration and the faster carrier mobility in operational devices. A linearly increasing voltage in reverse bias was applied to the film, as shown in **Figure 2**a. The response of the circuit has two components: an initial step due to the displacement current, charging the capacitor (j_0), and an additional conduction current forming a maximum at time t_{max}, due to extraction of equilibrium charge carriers. Carrier mobility was then calculated using t_{max}, as previously shown.[35] In Figure 2a, the intense patterned area represents capacitive charging while the sparse patterned area corresponds to extraction of the equilibrium charge carriers Q_0. It should be noted that to obtain Q_0, the integration should be done from zero time to the time at which the extraction current decreases to the displacement current. Another possibility to estimate the equilibrium amount of charge is from the initial slope of the current transient as described elsewhere.[34] The calculated doping level (in terms of the mobile charge carrier concentration) is

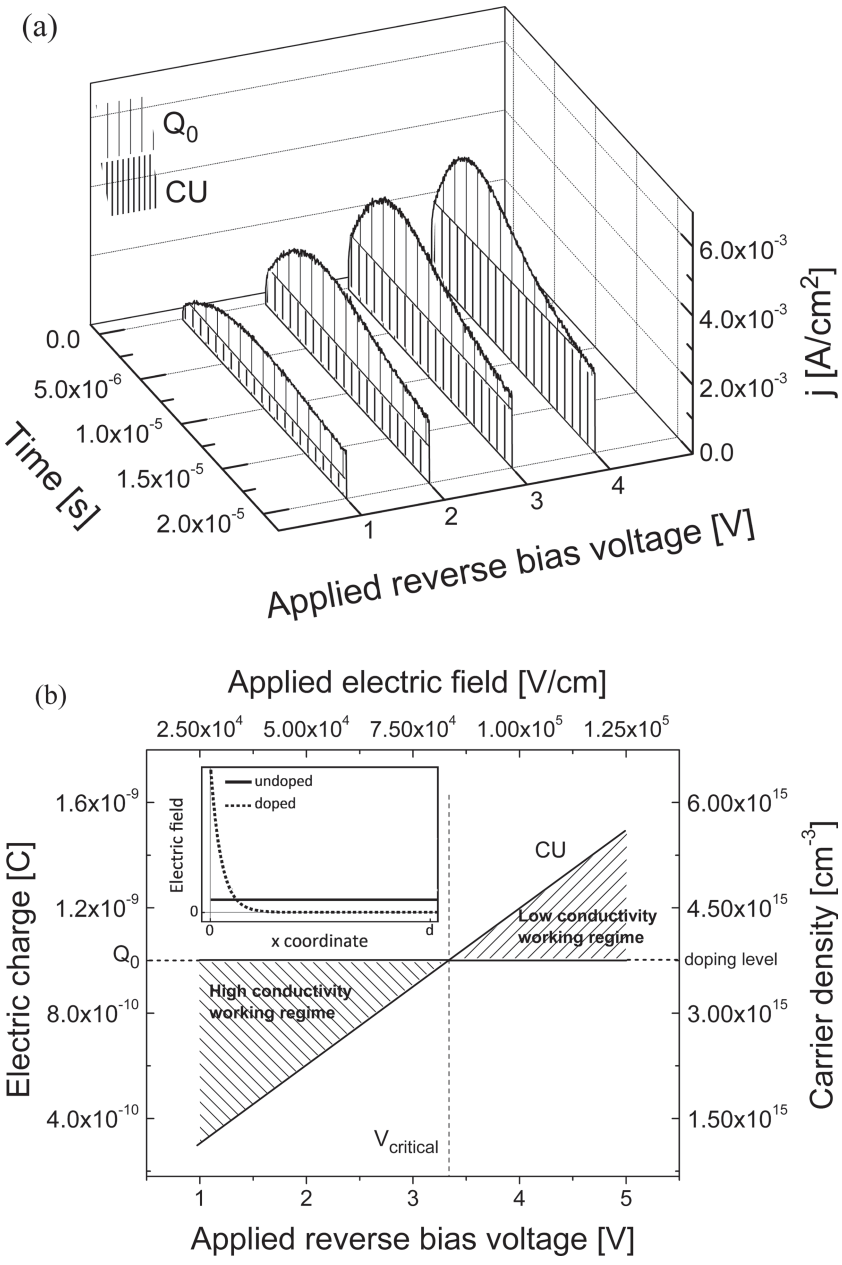

Figure 2. (a) Experimentally measured dark CELIV current density transients in doped P3HT:PCBM devices shown at various reverse bias triangle voltages demonstrating the transition from high to low conductivity working regimes as seen from the ratio of $\frac{Q_0}{CU}$, where the doping-induced mobile charge Q_0 is shown as the sparse pattern and the total charge on the electrodes CU is shown as the dense pattern (C is the capacitance of the device and U the peak voltage of the applied triangle pulse). (b) demonstrates the transition from low conductivity to high conductivity working regimes as a function of applied external voltage in reverse bias. At low voltages, the charge CU is less than the amount of equilibrium doping-induced charge carriers which corresponds to the high conductivity working regime where the electric field is screened by equilibrium charge carriers. At high voltages, CU is higher than the equilibrium charge which is considered as the low conductivity regime. The graph demonstrates the critical electric field at which the two regimes are separated. Inset: idealized schematic electric field profile inside the device for very low and very high conductivity materials (the x-coordinate indicating depth through the active layer). The graph demonstrates the screening of the electric field by free charge carriers in high conductivity material (doped) where the electric field vanishes dramatically in the device. In low conductivity material the electric field remains unscreened which can be the case in a thin film solar cell or in a solar cell with a large reverse bias voltage.

DOI: 10.1002/aenm.201200581

estimated to be 5×10^{15} cm^{-3} in the studied films. By changing the applied voltage, we varied CU without changing Q_0, thereby swapping between the two conductivity regimes. At low triangle voltages U_m, we find that CU is less than Q_0, so the transit time t_{tr} is greater than the dielectric relaxation time τ_σ and the high conductivity regime applies. In contrast, at high U_m, CU is greater than Q_0 (and $t_{tr} < \tau_\sigma$) which means the working regime is that of low conductivity. This is clearly shown in Figure 2b by plotting Q_0 and CU as a function of the electric field (or applied external voltage). At the specific voltage (electric field), $V_{critical}$ ($E_{critical}$), this transition occurs when CU becomes equal to Q_0. Changing the working regime from high to low conductivity by increasing the applied voltage is equivalent to varying the doping level from high to low respectively. In practice, controlling the doping level of organic semiconductors by modifying the properties of the materials is extremely difficult, so this electrical control method is very convenient. In the inset of Figure 2b, the electric field profile is shown schematically. The field is screened in the more highly doped device where the depletion layer is narrow compared to the field-free region (high conductivity). It is minimally screened in the low conductivity case wherein the doping level is low or the reverse bias voltage is high enough for the depletion layer to cover the whole thickness of the film.

The working regimes discussed above are important for interpreting the DI transients because one needs to be aware of the conductivity regime in order to choose the correct formula for calculating the bimolecular recombination. It is also worth noting that important information concerning carrier transport and recombination, typically inaccessible by classical time-of-flight (ToF) methods in operational devices because of significant doping levels,[16] can be obtained by applying this double injection transient technique.[34]

As shown in **Figure 3**, the DI current transients closely resemble the analytical transients for non-Langevin bimolecular recombination shown in Figure 1 and demonstrate strongly increasing injection current due to the charge carrier accumulation, with saturation to a steady state current.[34,36] At low forward bias voltages U_{FB}, a minimum in the current transients is determined by the Ohmic injection current, j_σ and trapping, which can be observed from slightly decaying injection current at the beginning of the transient signal.[36] At high U_{FB}, the minimum is determined by the space charge limited current (SCLC). The "kink" marked as stars and circles in Figure 3, is measured from the maximum of the derivative of the transient signal and it represents either the transit time of slower carriers, t_{slow} (in the case of the low conductivity working regime, high applied external voltage) or the transit time of minority carriers (in the case of the high conductivity working regime, low applied external voltages). Ambipolar (minority) carrier transit time in the case of the high conductivity regime is influenced by the trapping,[36] therefore the ambipolar carrier transit time and mobility estimation in this case is not straightforward and would lead to underestimated mobility values.

Using the CELIV and DI current transients the charge carrier mobilities and bimolecular recombination coefficients can be calculated as a function of applied electric field which is equivalent to scanning across the conductivity regimes. The minority

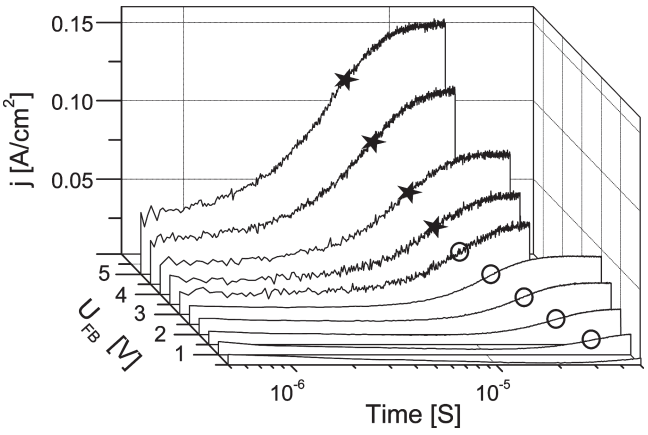

Figure 3. Double injection current density transients measured in P3HT:PCBM devices at various applied forward bias voltages U_{FB}. The stars mark the transit time t_{slow} of slower carriers (in the case of the low conductivity working regime, high applied external voltage) and the circles represent t_m which corresponds to the ambipolar transit time (in the case of the high conductivity working regime, low applied external voltages) which can only be clearly observed in the derivative, as explained in Figure 1. However, these ambipolar transit times were not used to calculate the ambipolar mobilitiesduetothe significant charge carrier trapping at low applied voltages.

and majority carrier mobilities as a function of square root of the electric field are shown in **Figure 4**a and are found to be equal. Majority carrier mobility was directly calculated from the dark-CELIV current maximum (t_{max}) in Figure 2a (for details please see citation).[35] It is essential to note that the electric field is not constant in a CELIV experiment since the voltage is linearly increasing. Therefore, an exact functional dependence cannot be determined unambiguously. However, an approximate trend can be extracted. We use the electric field at t_{max} where the strongest extraction occurs ($E = At_{max}/d$ where A is the triangle slope). It is clear from Figure 4a that the majority carrier mobility does not strongly depend on the electric field. The minority carrier mobility is measured from the slower carrier transit time obtained from the DI transients for the low conductivity regime using equation[34]

$$\mu_{\min} = 0.75 \frac{d^2}{t_{slow} U_{FB}} \tag{8}$$

In Figure 4b, β_L/β is plotted as a function of applied voltage (electric field). We used the photo-CELIV[30] technique (dashed line) to confirm the results of the DI experiments in both low and high conductivity regimes [Equations (3) and (7) respectively] with excellent agreement. This correlation confirms that at these levels of doping the bimolecular recombination is not changed and it is still lower compared to the Langevin recombination by two orders of magnitude even when the width of the field-free region is varied by the reverse bias. However, efficient charge collection depends on the product of the slower carrier mobility (μ_{slower}) and the bimolecular recombination reduction factor β_L/β.[13] The calculated minimum value of this product for good charge collection is $\mu_{slower}\beta_L/\beta|_{critical-minimum} = 4.3 \times 10^{-3} cm^2/Vs$, using

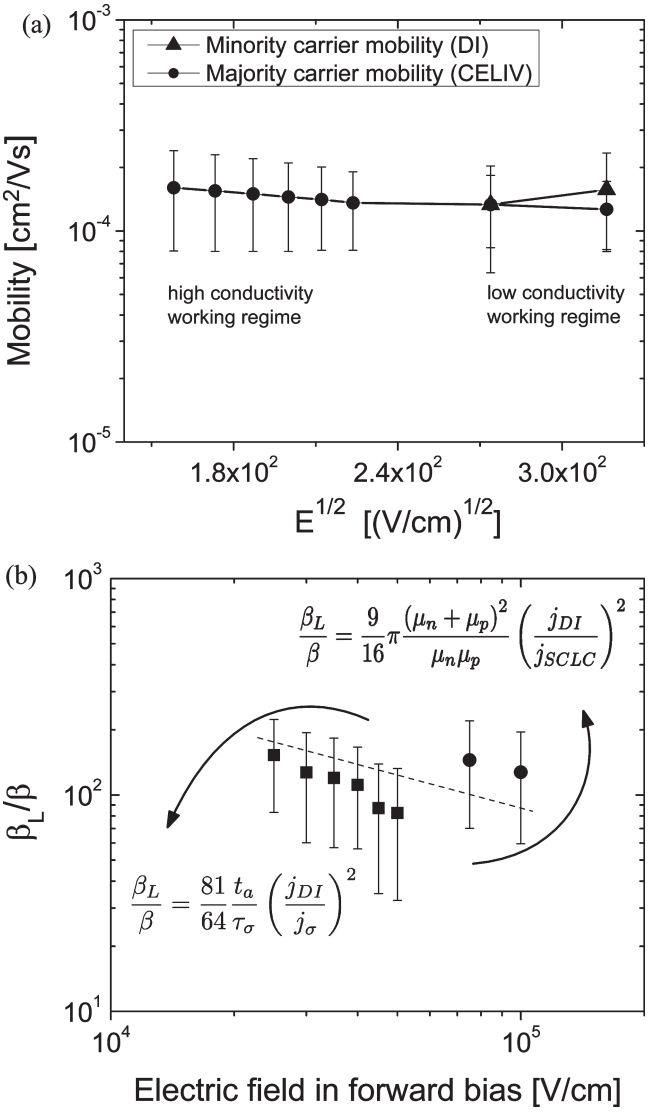

Figure 4. (a) Majority and minority carrier mobilities shown as a function of the square root of the electric field in moderately doped P3HT:PCBM solar cells measured from majority and minority carrier transit times respectively obtained from CELIV and DI transients. Mobilities were measured using dark CELIV (Figure 2a) and double injection transients (Figure 3) and are seen to be electric field independent. The minority carrier mobility was found to be almost equal to the majority carrier mobility. (b) Bimolecular recombination reduction factor β_L/β calculated using double injection Equation (3) (rectangles) and Equation (7) (circles) shown as a function of electric field. Dashed line shows the value estimated by photo-CELIV. The results indicate that in the moderately doped P3HT:PCBM solar cell the bimolecular recombination is still strongly suppressed compared to the Langevin limit, while the measurement error does not allow one to derive an exact functional dependence.

Equation (12) from citation,[16] and the parameters PCE = 3.2%, $Uoc = 0.6\ V$, $FF = 0.6$, $\varepsilon = 3.8$ and $d = 390$ nm. The actual value $\mu_{slower}\beta_L/\beta|_{actual} = 0.014\ cm^2/Vs$ is calculated using the estimated slower carrier mobility from Figure 4a under operational conditions (the built-in field) and the bimolecular recombination reduction factor from Figure 4b. The fact that the value of $\mu_{slower}\beta_L/\beta|_{actual}$ is much larger than $\mu_{slower}\beta_L/\beta|_{critical-minimum}$ shows that the performance is not limited by charge collection efficiency and therefore not hindered by the electric field screening induced by doping. This is an important and somewhat unexpected insight.

4. Conclusion

In summary, double injection transient, photo- and dark-CELIV techniques have been utilized to investigate charge transport and recombination in moderately doped operational P3HT:PCBM bulk-heterojunction organic solar cells. Using dark-CELIV, an equilibrium charge carrier concentration of $n = 5 \times 10^{15}$ cm^{-3} and a weakly electric field dependent majority carrier mobility of approximately $10^{-4} cm^2/Vs$ were determined and were shown to be equal to the minority carrier mobility from double injection measurements. We have shown that the working regime of moderately doped organic solar cells can be adjusted to represent either high or low conductivity modes, which are responsible for determining the photocurrent-governing mechanism through diffusion or drift respectively. An analytical theory to calculate the bimolecular recombination coefficients in both regimes from double injection is derived and it agrees well with experiment. Applying the theory to our experimental results for both regimes we find that the recombination coefficient obtained from the double injection technique is in a good agreement with the photo-CELIV method. Strongly non-Langevin carrier recombination ($\beta_L/\beta = 145$) is observed in these moderately doped devices which shows that partial electric field screening does not significantly hinder the charge collection in operational P3HT:PCBM solar cells since the product of slower carrier mobility and the bimolecular recombination reduction factor is large enough to provide high charge collection efficiency.

5. Experimental Section

Standard BHJ poly(3-*n*-hexylthiophene):phenyl-C61-butyric acid methyl ester (P3HT:PC60BM) solar cells were prepared as follows: 15 Ω/sq. indium tin oxide coated glass substrates (Kintec) patterned by photolithography were cleaned by sonicating in sequence with Alconox (detergent), de-ionized water, acetone and *iso*-propanol for 10 minutes. The cleaned substrates were coated with a 20 nm layer of poly(3,4-ethylenedioxythiophene) doped with poly(styrene sulfonate) (PEDOT:PSS) by spin casting at 5000 rpm for 60 sec. The PEDOT:PSS layer was baked for 10 min at 170 °C. A solution of poly(3-*n*-hexylthiophene) (Merck, RR 94.6%, Mw = 111,800) and phenyl-C61-butyric acid methyl ester (Nano-C) with a mass ratio of 1:1 was prepared at a total concentration of 40 mg/cm^3 in anhydrous 1,2-dichlorobenzene (DCB) and deposited on top of the PEDOT:PSS layer after filtration by spin coating at 600 rpm for 80 sec. This resulted in a 390 nm thick bulk heterojunction layer as measured by a Veeco Dektak150 profilometer. Slow drying was performed after spin coating for 2 hours by placing the coated film in a partially opened petri dish. Finally a 100 nm aluminum layer was deposited to complete the device by thermal evaporation under a 10^{-6} mbar vacuum. The device area was 0.038 cm^2 with three devices per substrate. An average power conversion efficiency of 3.2. ± 0.1% (out of 6 devices) under simulated AM1.5G (1000 W/m^2) illumination was obtained after 2 minutes annealing at 170 °C. This is typical of the performance of P3HT:PCBM cells at this thickness produced in our laboratory.

DOI: 10.1002/aenm.201200581

Photo-CELIV was performed using a pulsed third-harmonic Nd:YAG laser (Quantel Brio) working at a wavelength of 355 nm and pulse duration of 5 ns. The laser beam was attenuated by a neutral density filter set. A delay generator (Stanford Research System DG535) and an arbitrary waveform generator (Agilent 33250A) were used to generate the CELIV triangle pulse with adjustable voltage slope and time delay. The signal was recorded by a digital storage oscilloscope (LeCroy Waverunner A6200). The details of measuring the bimolecular recombination using photo-CELIV are described in detail in the references.[30,35]

Acknowledgements

A.P. is the recipient of an Australian Research Council Discovery Early Career Researcher Award (Projects: ARC DECRA DE120102271, UQ ECR59-2011002311 and UQ NSRSF-2011002734). P.M. and P.L.B. are a Vice Chancellor's Senior Research Fellows. A.A. is funded by a University of Queensland International scholarship (UQI). B.P. is funded by an Australian Postgraduate Award (APA). We acknowledge funding from the University of Queensland (Strategic Initiative–Centre for Organic Photonics & Electronics), the Queensland Government (National and International Research Alliances Program) and the ARC Centre of Excellence for Antimatter-Matter Studies. This work was performed in part at the Queensland node of the Australian National Fabrication Facility (ANFF) - a company established under the National Collaborative Research Infrastructure Strategy to provide nano and microfabrication facilities for Australia's researchers.

Received: July 31, 2012
Published online:

[1] G. Yu, J. Gao, J. Hummelen, F. Wudl, A. Heeger, *Science* **1995**, *270*, 1789.
[2] C. J. Brabec, S. Gowrisanker, J. J. M. Halls, D. Laird, S. Jia, S. P. Williams, *Adv. Mater.* **2010**, *22*, 3839.
[3] C. Deibel, V. Dayakonov, *Rep. Prog. Phys.* **2010**, *73*, 096401.
[4] W.-Y. Lai, M. l. N. Balfour, J. W. Levell, A. K. Bansal, P. L. Burn, S.-C. Lo, I. D. W. Samuel, *Macromolecules* **2012**, *45*, 2963.
[5] M. Aljada, A. K Pandey, M. Velusamy, P. L Burn, P. Meredith, E. B. Namdas, *J. Phys. D: Appl. Phys.* **2012**, *45*, 225105.
[6] A. J. Clulow, P. L. Burn, P. Meredith, P. E. Shaw, *J. Mater. Chem.* **2012**, *22*, 12507.
[7] S. H. Park, A. Roy, S. Beaupre, S. Cho, N. Coates, J. S. Moon, D. Moses, M. Leclerc, K. Lee, A. J. Heeger, *Nat. Phot.* **2009**, *3*, 297.
[8] T.-Y. Chu, S.-W. Tsang, J. Zhou, P. G. Verly, J. Lu, S. Beaupre, M. Leclerc, Y. Tao, *Sol. Energy Mater. Sol. Cells* **2012**, *96*, 155.
[9] J. H. Seo, A. Gutacker, Y. Sun, H. Wu, F. Huang, Y. Cao, U. Scherf, A. J. Heeger, G. C. Bazan, *J. Am. Chem. Soc.* **2011**, *133*, 8416.
[10] Z. Liang, A. Nardes, D. Wang, J. J. Berry, B. A. Gregg, *Chem. Mater.* **2009**, *21*, 4914.
[11] J. Schafferhans, A. Baumann, A. Wagenpfahl, C. Deibel, V. Dyakonov, *Org. Electron.* **2010**, *11*, 1693.
[12] A. Liu, S. Zhao, S.-B. Rim, J. Wu, M. Konemann, P. Erk, P. Peumans, *Adv. Mater.* **2008**, *20*, 1065.
[13] C. K. Chan, W. Zhao, A. Kahn, I. G. Hill, *Appl. Phys. Lett.* **2009**, *94*, 2033306.
[14] T. Taima, J. Sakai, T. Yamanari, K. Saito, *Sol. Energy Mater. Sol. Cells* **2009**, *93*, 742.
[15] W. L. Leong, G. C. Welch, L. G. Kaake, C. J. Takacs, Y. Sun, G. C. Bazan, A. J. Heeger, *Chem. Sci.* **2012**, *3*, 2103.
[16] A. Pivrikas, H. Neugebauer, N. S. Sariciftci, *IEEE J. Sel. Top. Quantum Electron.* **2010**, *16*, 1746.
[17] A. J. Morfa, A. M. Nardes, S. E. Shaheen, N. Kopidakis, J. van de Lagemaat, *Adv. Funct. Mater.* **2011**, *21*, 2580.
[18] G. Garcia-Belmonte, A. Munar, E. M. Barea, J. Bisquert, I. Ugarte, R. Pacios, *Org. Electron.* **2008**, *9*, 847.
[19] E. J. Meijer, A. V. G. Mangnus, B.-H. Huisman, G. W. 't Hooft, D. M. de Leeuw, T. M. Klapwijk, *Synth. Met.* **2004**, *142*, 53.
[20] L. J. A. Koster, V. D. Mihailetchi, H. Xie, P. W. Blom, *Appl. Phys. Lett.* **2005**, *87*, 203502.
[21] L. Liu, G. Li, *Sol. Energy Mater. Sol. Cells* **2011**, *95*, 2557.
[22] D. Rauh, C. Deibel, V. Dyakonov, *Adv. Funct. Mater.* **2012**, *22*, 3371.
[23] G. Juška, K. Arlauskas, J. Stuchlik, R. Österbacka, *J. Non-Cryst. Solids* **2006**, *352*, 1167.
[24] A. J. Mozer, N. S. Sariciftci, A. Pivrikas, R. Österbacka, G. Juška, L. Brassat, H. Bässler, *Phys. Rev. B* **2005**, *71*, 035214.
[25] A. Pivrikas, G Juška, A. J. Mozer, M. Scharber, K. Arlauskas, N. S. Sariciftci, H. Stubb, R. Österbacka, *Phys. Rev. Lett.* **2005**, *94*, 176806.
[26] T. Daeneke, Y. Uemura, N. W. Duffy, A. J. Mozer, N. Koumura, U. Bach, L. Spiccia, *Adv. Mater.* **2012**, *24*, 1222.
[27] D. Credgington, J. R. Durrant, *J. Phys. Chem. Lett.* **2012**, *3*, 1465.
[28] A. Pivrikas, N. S. Sariciftci, G. Juška, R. Österbacka, *Prog. Photovolt. Res. Appl.* **2007**, *15*, 677.
[29] T. M. Clarke, J. Peet, P. Denk, G. Dennler, C. Lungenschmied, A. J. Mozer, *Energy Environ. Sci.* **2011**, *5*, 5241.
[30] N. Nekrašas, K. Genevičius, M. Viliūnas, G. Juška, *Chem. Phys.* **2012**, *404*, 56.
[31] M. A. Lampert, P. Mark, *Current Injection in Solids*, Academic Press, New York and London, **1970**.
[32] N. F. Mott, R. W. Gurney, *Electronic processes in ionic crystals (2nd ed.)*, Oxford University Press, London, **1948**.
[33] A. M. Lampert, A. Rose, *Phys. Rev.* **1961**, *121*, 26.
[34] G. Juška, K. Geneviius, G. Sliaužys, A. Pivrikas, M. Scharber, *J. Appl. Phys.* **2007**, *101*, 114505.
[35] G. Juška, K. Arlauskas, M. Viliūnas, R. Österbacka, H. Stubb, *Phys. Rev. B.* **2000**, *62*, 235.
[36] G. Juška, K. Geneviius, G. Sliaužys, N. Nekrasas, R. Österbacka, *J. Non-Cryst. Solids* **2008**, *354*, 2858.